SEQUENTIAL LOW RANK REPRESENTATION FOR BLOOD GLUCOSE MEASUREMENTS

Karim Wahby

Technische Universität Darmstadt
Darmstadt, Germany
wahby.karim@gmail.com

Nevine Demitri and Abdelhak M. Zoubir

Signal Processing Group
Technische Universität Darmstadt
Darmstadt, Germany
{ndemitri, zoubir}@spg.tu-darmstadt.de

ABSTRACT

We propose using the Low Rank Representation (LRR) method for segmentation of video frames of glucose concentration measurements taken by a novel setup intended for use in a hand-held device. We propose a sequential LRR algorithm, that corrects the error in the data matrix at each point in time and uses it calculate an f data matrix for the next step. By fixing the error in the data, we are able to segment the data using fewer number of frames at an early stage of the chemical reaction. Our aim is to process incoming frames taken by the camera in real time and use them in a sequential manner to segment the images and estimate the feature value of the region of interest. A comparison of standard LRR and sequential LRR is presented. We evaluate both algorithms on real data sets with respect to goodness of segmentation, as well as accuracy of the feature estimates.

Index Terms— Low Rank Representation, spectral clustering, image segmentation, glucose measurement, photometry

1. INTRODUCTION

According to the WHO statistics [1], 1.5 million deaths are directly related to diabetes each year. Currently 9% of the worlds population have diabetes. Diabetes is a long term disease which has a direct effect of the increase in blood glucose concentration [1, 2]. Today, a wide range of hand-held blood sugar measurement devices are available for purchase and enable self-monitoring by the patient.

We consider data obtained from an invasive, hand-held device, that utilizes a novel photometric measurement principle requiring a much smaller blood sample than the state-of-the-art devices [3]. Accuracy of the hand-held devices is very crucial for the patient, as the patient will be prescribed a certain amount of medication depending on the blood sugar level indicated by the device. To measure the blood sugar level, the patient extracts a small blood sample, typically from the finger. The blood sample is applied to a test strip, which carries a chemical substance that reacts with the glucose in blood and changes its color. The color change is directly related to the underlying glucose concentration and is measured in terms of the reflected light, referred to as *relative remission*. A camera captures the chemical reaction taking place on the test strip in the form of video frames. Using methods to segment these images [3, 4], we are able to identify the Region of Interest (ROI). The ROI is the area, where the blood sample has been placed and the chemical reaction takes place. The intensity of the ROI is mapped directly to an estimate of the underlying glucose concentration. Figure 1 presents examples of the chemical reaction captured at different time instances. In Fig. 1(a) the reaction has not started yet and no change in relative remission value over the test strip is visible, but rather a very homogenous reflectivity. In Fig. 1(b) and (c), as we advance in time, the reaction is taking place and the relative remission value is decreasing in the ROI. Figure 1(d) shows the saturation of the reaction and the ROI, where the color change is clearly identifiable in contrast to surrounding areas, where a much weaker color change is observable. Low Rank Representation (LRR) [5, 6] is used to segment data drawn from a union of multiple subspaces. Using one subspace to describe the whole data is rarely enough [5, 6]. The more reasonable approach is to consider the data lying in multiple subspaces; that is all samples are drawn from a mixture of low-rank subspaces. Subspace segmentation [7] is a challenging problem that aims at clustering the data into groups with each group corresponding to a subspace, while correcting possible errors. It has been applied in different fields such as computer vision [8], [9], [10], image processing [11], [12]

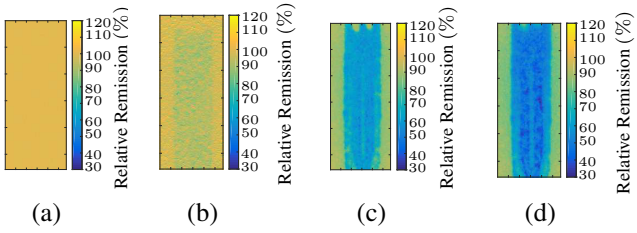

Fig. 1. Examples of observed images at different time instants: (a) $t = 0\,\mathrm{s}$, (b) $t = 0.3\,\mathrm{s}$, (c) $t = 5\,\mathrm{s}$, (d) $t = 18\,\mathrm{s}$.

978-0-9928-6265-7/16/$31.00 ©2016 IEEE

and system identification [13].
In this paper we apply the LRR subspace segmentation method for segmentation of blood sugar images. In our application the images arrive sequentially over time and we want to take advantage of this property. In [14] a sequential LRR is presented that introduces a smoothing term in the optimisation problem to convey the smoothness of sequential data. However, the processing of the data in this work is done in batches. Our work is different in the sense that we apply the standard LRR algorithm to deal with data arriving sequentially. We correct the incoming data from errors by subtracting the error term calculated using the previous frames. We make use of the fact, that the relative remission of different areas of the test strip change with varying strength. We assume that our test strip shows three regions: the region, where the chemical reaction takes place; the test strip itself, where there is no chemical reaction taking place; and a transition area between both regions that exhibits a much weaker change in relative remission. As we advance in time the relative remission of the regions, where the reaction takes place changes faster than that of the neighbouring areas. This motivates the assumption of a union of subspaces.
Our contribution lies in applying LRR to the glucose image segmentation problem. Furthermore, we propose a novel sequential LRR that corrects the error in the data as we proceed through time. We evaluate both approaches using a real data set.
The remainder of the paper is organized as follow: Section 2 introduces the LRR principle. The sequential LRR algorithm is described in Sec. 3. Section 4 introduces our data set and discusses the results. Finally a conclusion is given in Sec. 5.

2. LOW RANK REPRESENTATION

2.1. Problem Statement

Low Rank Representation (LRR) [5, 6] is used for the segmentation of a union of multiple linear (or affine) subspaces. Given a set of data vectors, that are drawn from a union of multiple subspaces, the LRR algorithm aims to find the lowest rank matrix that represents the data vectors as a linear combination of others. LRR is different from other compression techniques such as Sparse Representation (SR), [15] in the sense that it considers all the data jointly. After finding the lowest rank matrix, a so-called affinity matrix is calculated that is used to define an undirected graph and is fed to a spectral clustering algorithm such as Normalized Cuts (NCuts) [16]. In the sequel, we will give a short presentation of the LRR optimisation problem.
Following notation will be used for the remainder of this paper: $\mathbf{X}$ will denote a matrix with the ij-th element given by x_{ij}. Vectors will be given by $\mathbf{x}$, while x is used for scalar quantities and X for constants.

2.2. Low Rank Representation

Let $\mathbf{X} = \left[\mathbf{x}_1, \mathbf{x}_2, \ldots, \mathbf{x}_N\right] \in \mathbb{R}^{M\times N}$ be a set of N data vectors, where each data vector $\mathbf{x}_i$ represents a sample and M is the dimension of each data vector. We assume that the data vectors are drawn from a union of k subspaces $\{S_i\}_{i=1}^{k}$, which can be represented by a linear combination of vectors of the dictionary $\mathbf{A} = \left[\mathbf{a}_1, \mathbf{a}_2, \ldots, \mathbf{a}_N\right] \in \mathbb{R}^{M\times N}$. The LRR problem is given by the following minimisation problem [5,6]

$$\begin{aligned} \underset{\mathbf{Z}}{\text{minimize}} \quad & \text{Rank}\big(\mathbf{Z}\big), \\ \text{subject to} \quad & \mathbf{X} = \mathbf{A}\mathbf{Z}, \mathbf{A} = \mathbf{X}. \end{aligned} \tag{1}$$

Here $\mathbf{Z} = \left[\mathbf{z}_1, \mathbf{z}_2, \ldots, \mathbf{z}_N\right]$ is a coefficient matrix with each vector $\mathbf{z}_i$ containing the low-rank representation of $\mathbf{x}_i$. The low-rankness is a more suitable criterion for retrieving the global structure in the data, compared to sparse representation [5, 6]. The low-rank representation uses the self-expressiveness property, making use of the data to represent itself while maintaining the global structure of the data. The optimal solution to Eq. (1), denoted by $\mathbf{Z}^*$, is now called the lowest rank representation of $\mathbf{X}$ given a certain dictionary $\mathbf{A}$. The dictionary is given here by the data itself $\mathbf{A} = \mathbf{X}$. It is intuitive for clustering and segmentation applications to express the data by itself. To overcome the computational difficulty of the rank problem in Eq. (1), matrix completion methods [17–19] are adopted and the problem in Eq. (1) reduces to minimising the nuclear norm of $\mathbf{Z}$. The optimisation problem now reads

$$\begin{aligned} \underset{\mathbf{Z}}{\text{minimize}} \quad & \|\mathbf{Z}\|_*, \\ \text{subject to} \quad & \mathbf{X} = \mathbf{X}\mathbf{Z}, \end{aligned} \tag{2}$$

where $\|\|_*$ is referred to as the nuclear norm [20].
Since in real applications the presence of noise, and in our case also outliers, must be taken into consideration, Eq. (2) needs to be adjusted. This results in following formulation that is appended a regularization term to compensate for the error

$$\begin{aligned} \underset{\mathbf{Z},\mathbf{E}}{\text{minimize}} \quad & \|\mathbf{Z}\|_* + \lambda\|\mathbf{E}\|_l, \\ \text{subject to} \quad & \mathbf{X} = \mathbf{X}\mathbf{Z} + \mathbf{E}, \end{aligned} \tag{3}$$

where $\|\cdot\|_l$ denotes e.g. the $l_{2,1}$ norm, used to deal with sparse sample specific corruptions or the Frobenius norm, which deals with Gaussian noise [21]. They are given by

$$\begin{aligned} l_{2,1}\text{ norm} \qquad & \|\mathbf{E}\|_{2,1} = \sum_{j=1}^{m}\sqrt{\sum_{i=1}^{n}|e_{ij}|^2} \\ \text{Frobenius norm} \quad & \|\mathbf{E}\|_F = \sqrt{\sum_{i=1}^{n}\sum_{j=1}^{m}|e_{ij}|^2} \end{aligned}$$

The parameter λ is used to tune the effect of the error term and it can be found empirically in the range $0 < \lambda < 1$. The

optimisation problem is solved using the inexct-Augmented Lagrange Multiplier method (inexact-ALM) [22]. Given the coefficient matrix $\mathbf{Z}$ and the error matrix $\mathbf{E}$, we want to segment the data into the corresponding subspaces. For that, we need to construct an affinity matrix [5, 6], that includes affinities between the data vectors. The low-rank structure obtained by $\mathbf{Z}$ is used to define an affinity matrix and fed into a spectral clustering algorithm as described in [6].

3. SEQUENTIAL LOW RANK REPRESENTATION

As we advance in time, more frames are obtained by the photometric measurement setup discussed in [3], representing the data vectors in our application. Our understanding of sequential processing is processing the captured frames sequentially as we advance through time. We perform LRR at each point in time, always obtaining an error term, that describes the error of the current data matrix. This is subtracted from the current data matrix to correct it. The data matrix to be used in the next step is error-removed, according to the LRR outcome.

We denote by n a certain point in time such that $n = 1, \ldots, N$, and N is the total number of frames captured. Each new incoming frame at time n is given by $\mathbf{F}_n \in \mathbb{R}^{K \times L}$, where K and L are the number of rows and columns, respectively. A frame $\mathbf{F}_n$ is first vectorised,

$$\mathbf{f}_n = \text{vec}\big(\mathbf{F}_n\big),$$

where $\mathbf{f}_n \in \mathbb{R}^{1 \times M}$ and $M = K \times L$. The resulting data matrix before removing the error at time n is $\mathbf{X}_n = [\mathbf{f}_1, \ldots, \mathbf{f}_n]^T$. As explained in Sec. 2.2, we use the data itself as the dictionary.

At each point n in time the standard LRR problem is solved using $\tilde{\mathbf{X}}_n = [\hat{\mathbf{X}}_{n-1}; \mathbf{f}_n^T]$, where $\hat{\mathbf{X}}_{n-1}$ is the error-removed data matrix at the previous time instance $n-1$. The LRR results in two matrices:

1. The lowest-rank representation matrix $\mathbf{Z}_n$, and
2. the error matrix $\mathbf{E}_n$.

As a final step the current error $\mathbf{E}_n$ is subtracted from the data matrix, such that it becomes

$$\hat{\mathbf{X}}_n = \tilde{\mathbf{X}}_n - \mathbf{E}_n.$$

The process is repeated until the final frame is received and the data can be segmented. We use $\mathbf{Z}_N$, i.e. the final computed coefficient matrix, to construct the affinity matrix as explained in Sec. 2. The affinity matrix is then fed to spectral clustering algorithm as presented in [15]. The proposed sequential LRR algorithm is presented in Algorithm 1.

Algorithm 1 Sequential Low Rank Representation

Input: $\{\mathbf{f}_1, \ldots, \mathbf{f}_N\}$
Output: $\mathbf{Z}_N, \mathbf{E}_N$ and segmented images

1: **for** Each new incoming frame $\mathbf{f}_n$ **do**
2: $\quad \tilde{\mathbf{X}}_n = [\hat{\mathbf{X}}_{n-1}; \mathbf{f}_n^T]$ ▷ Update data vector to include the incoming frame
3: $\quad \mathbf{Z}_n, \mathbf{E}_n$ ▷ Perform LRR as in Eq. (3) using $\mathbf{X} = \tilde{\mathbf{X}}_n$
4: $\quad \hat{\mathbf{X}}_n = \tilde{\mathbf{X}}_n - \mathbf{E}_n$. ▷ Remove calculated error from the data
5: **end for**
6: $\mathbf{Z}_N, \mathbf{E}_N$ ▷ Perform LRR as in Eq. (3) using $\mathbf{X} = \tilde{\mathbf{X}}_N$
7: Construct affinity matrix using $\mathbf{Z}_N$ [5, 6]
8: Segment using spectral clustering as in [15]

4. EXPERIMENTAL RESULTS

4.1. Data Set & Measurement Setup

We use a real data set consisting of 81 measurements. The measurements are taken using the photometric measurement device described in [3]. Whole blood samples of different glucose concentrations ranging between 30 mg/dl to 550 mg/l are used. Each measurement contains $N = 582$ frames, corresponding to a testing time $t_{\text{test}} = 19.4\,\text{s}$. The images are preprocessed as in [3]. The regularization parameter is set to $\lambda = 0.15$ and the Frobenius norm is used for the error term.

4.2. Results

Using the real data we perform two different analysis:

1. Batch Processing: each measurement video consisting of $N = 582$ frames is processed as a batch. We denote this: standard LRR [5, 6].
2. Sequential Processing: the set of $N = 582$ frames is processed sequentially, as described in Algorithm 1. We denote this: sequential LRR.

After segmenting the images, we calculate the mean of the relative remission value of each segmented area in the image. The ROI is identified as the area with the lowest relative remission value. We take this value to be the estimate of the relative remission $\widehat{R}$.

We set our algorithm to consider one frame every $t_{\text{skip}} = 1/10\,\text{s}$, which is equivalent to skipping 3 captured frames. We start with the evaluation of the standard LRR batch processing. We expect that as the glucose concentration in blood increases the relative remission estimate $\widehat{R}$ decreases. The reason for this is the more glucose contained in the blood sample, the stronger the reaction with the test strip and the stronger the color change with respect to the initial color of the chemical test strip. Figure 2 (a) depicts the ground truth of glucose concentrations (GC) versus the estimated remission values using standard LRR. In Fig. 2 (a) it is clear that $\widehat{R}$ meets the expected behaviour. Now that we have established that LRR

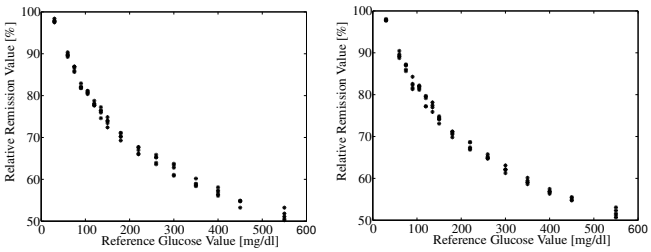

(a) Standard LRR (b) Sequential LRR

Fig. 2. Relative Remission estimates obtained using (a) Standard LRR and (b) Sequential LRR.

method is applicable to our dataset we evaluate the proposed sequential LRR algorithm. One advantage of sequentially

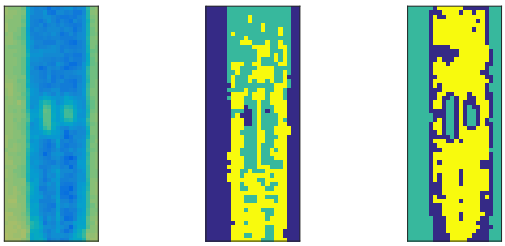

(a) (b) (c)

Fig. 3. (a) Original Image, (b) segmentation using standard LRR at frame $N = 582$, (c) segmentation using sequential LRR at frame $N = 200$.

processing the frames is that fewer number of frames is required to achieve correct segmentation, as compared to the batch processing. This comes from removing the error from the previously arriving data. We compare the outcome of the segmentation using only the first 200 frames using the sequential LRR, with the segmentation using the full video in the standard LRR case. Figure 3 (a) shows an original glucose image containing air bubbles in the ROI, which can be seen as outliers. The segmentation obtained by standard LRR (Fig 3 (b)) does not clearly identify the different regions of the image. Sequential (Fig 3 (c)) LRR on the other hand is able to correctly segment the image into different regions. The relative remission estimates $\widehat{R}$ are used here for evaluation and comparison. For the sequential LRR the segmentation of the ROI is identified from the segmentation at frame $N = 200$, while for the standard LRR frame $N = 582$ is used to identify the region of interest. In Fig. 2 (b) we can see clearly how the behaviour matches that of Fig. 2 (a). We are able to properly segment the images and determine the ROI while achieving similar results as the non-sequential approach, i.e., the standard LRR.

We investigate the accuracy of both cases of applying LRR to

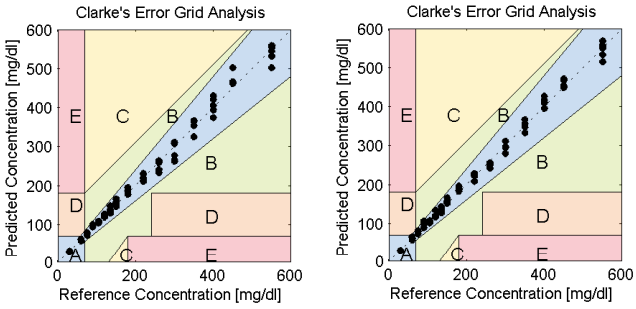

(a) Standard LRR (b) Sequential LRR

Fig. 4. Evaluation of accuracy using Clarke's Error Grid Analysis for (a) Standard LRR and (b) Sequential LRR.

GC in mg/dl	Seq. LRR	Stand. LRR	State-of-the-art
30	**0.15**	0.33	0.53
90	1.15	**0.47**	1.05
150	**0.90**	1.20	1.97
350	**0.95**	1.21	1.50
550	**1.83**	2.32	3.94

Table 1. Relative remission variation coefficient of $v_{\widehat{R}_i}$ for different glucose concentrations (GC) for the sequential LRR, the standard LRR, and the state-of-the-art mean-shift algorithm [24].

our dataset by drawing the Clarke Error Grids (CEG) [23]. The CEG plots the estimated glucose concentrations against the actual glucose concentrations and classifies the error according to its medical severity. Figure 4 depicts the ground truth glucose concentrations versus the estimated glucose concentrations. The estimated glucose concentrations are obtained using a predefined mapping function, with its argument being the estimated relative remission values $\widehat{R}$ [3]. Points in the CEG that fall in zones A, B are considered clinically accurate and indicate to the patient a correct course of treatment. On the contrary, measurements that fall in zones C, D and E are considered incorrect and they can lead to wrong treatment of the patient. Figure 4 shows the CEG analysis of both methods, i.e. standard and sequential LRR. It can be observed that for both methods all measurements fall in zones A and B, which indicates accurate results and non-harmful treatment for the patient. In Table 1 we list the relative remission variation coefficient $v_{\widehat{R}_i}$, which is calculated as follows. Let $\sigma_{\widehat{R}_i}$ be the standard deviation of the estimated relative remission values $\widehat{R}$ of a certain reference glucose level i and $\mu_{\widehat{R}_i}$ be the corresponding mean value. $v_{\widehat{R}}$ is defined as

$$v_{\widehat{R}_i} = \begin{cases} \sigma_{\widehat{R}_i} & \text{if } i \leq 100\,\text{mg/dl} \\ \frac{\sigma_{\widehat{R}_i}}{\mu_{\widehat{R}_i}} & \text{if } i > 100\,\text{mg/dl} \end{cases}$$

From Table 1 we see that the sequential LRR outperforms the standard LRR in terms of remission variance coefficient for

most cases. This can be attributed to the removal of the error in each step from the data. We also show that both standard LRR and sequential LRR outperform the state-of-the-art approach in [24].

5. CONCLUSION

We have presented two different low rank representation (LRR) approaches to segment blood glucose frames obtained by a novel photometric device: the standard LRR that processes the data in batches, and the sequential LRR that processes the data sequentially as it arrives. The sequential LRR estimates the error in the data at each time instant and removes it from the current data matrix. Both algorithms are evaluated using a real data set. We showed that the proposed sequential LRR algorithm is able to provide more accurate segmentations of the data using less frames. Furthermore, a comparison of the relative remission estimates of both the standard and sequential LRR show the superiority of the sequential LRR.

REFERENCES

[1] ," http://www.who.int/mediacentre/factsheets/fs312/en/(Retrieved January 2016).

[2] American Diabetes Association, "Diagnosis and classification of diabetes mellitus," *Diabetes Care*, vol. 37, no. Supplement 1, pp. S81–S90, 2014.

[3] N. Demitri and A.M. Zoubir, "Mean-shift based algorithm for the measurement of blood glucose in hand-held devices," in *2013 Proceedings of the 21st European Signal Processing Conference (EUSIPCO)*. IEEE, 2013, pp. 1–5.

[4] N. Demitri and A.M. Zoubir, "Estimating glucose concentration using a scalable sparse mean-shift algorithm," in *2015 IEEE 12th International Symposium on Biomedical Imaging (ISBI)*, April 2015, pp. 642–645.

[5] G. Liu, Z. Lin, and Y. Yu, "Robust subspace segmentation by low-rank representation," in *Proceedings of the 27th international conference on machine learning (ICML-10)*, 2010, pp. 663–670.

[6] G. Liu et al., "Robust recovery of subspace structures by low-rank representation," *IEEE Transactions on Pattern Analysis and Machine Intelligence*, vol. 35, no. 1, pp. 171–184, 2013.

[7] R. Vidal, "A tutorial on subspace clustering," *IEEE Signal Processing Magazine*, vol. 28, no. 2, pp. 52–68, 2010.

[8] S. Rao et al., "Motion segmentation in the presence of outlying, incomplete, or corrupted trajectories," *IEEE Transactions on Pattern Analysis and Machine Intelligence*, vol. 32, no. 10, pp. 1832–1845, 2010.

[9] J. Ho et al., "Clustering appearances of objects under varying illumination conditions," in *2003 IEEE Computer Society Conference on Computer Vision and Pattern Recognition*. IEEE, 2003, vol. 1, pp. I–11.

[10] G. Liu et al., "Unsupervised object segmentation with a hybrid graph model (hgm)," *IEEE Transactions on Pattern Analysis and Machine Intelligence*, vol. 32, no. 5, pp. 910–924, 2010.

[11] Y. Ma et al., "Segmentation of multivariate mixed data via lossy data coding and compression," *IEEE Transactions on Pattern Analysis and Machine Intelligence*, vol. 29, no. 9, pp. 1546–1562, 2007.

[12] M.A. Fischler and R.C. Bolles, "Random sample consensus: a paradigm for model fitting with applications to image analysis and automated cartography," *Communications of the ACM*, vol. 24, no. 6, pp. 381–395, 1981.

[13] C. Zhang and R.R. Bitmead, "Subspace system identification for training-based mimo channel estimation," *Automatica*, vol. 41, no. 9, pp. 1623–1632, 2005.

[14] Y. Guo et al., "Low rank sequential subspace clustering," in *2015 International Joint Conference on Neural Networks (IJCNN)*. IEEE, 2015, pp. 1–8.

[15] E. Elhamifar and R. Vidal, "Sparse subspace clustering," in *2009 IEEE Conference on Computer Vision and Pattern Recognition (CVPR)*. IEEE, 2009, pp. 2790–2797.

[16] J. Shi and J. Malik, "Normalized cuts and image segmentation," *IEEE Transactions on Pattern Analysis and Machine Intelligence*, vol. 22, no. 8, pp. 888–905, 2000.

[17] J. Cai, E.J. Candès, and Z. Shen, "A singular value thresholding algorithm for matrix completion," *SIAM Journal on Optimization*, vol. 20, no. 4, pp. 1956–1982, 2010.

[18] E.J. Candès and B. Recht, "Exact matrix completion via convex optimization," *Foundations of Computational mathematics*, vol. 9, no. 6, pp. 717–772, 2009.

[19] E.J. Candes and Y. Plan, "Matrix completion with noise," *Proceedings of the IEEE*, vol. 98, no. 6, pp. 925–936, June 2010.

[20] M. Fazel, *Matrix rank minimization with applications*, Ph.D. thesis, Stanford University, 2002.

[21] E. Elhamifar and R. Vidal, "Sparse subspace clustering: Algorithm, theory, and applications," *IEEE Transactions on Pattern Analysis and Machine Intelligence*, vol. 35, no. 11, pp. 2765–2781, 2013.

[22] Z. Lin, M. Chen, and Y. Ma, "The augmented lagrange multiplier method for exact recovery of corrupted low-rank matrices," *arXiv preprint arXiv:1009.5055*, 2010.

[23] W.L. Clarke et al., "Evaluating clinical accuracy of systems for self-monitoring of blood glucose," *Diabetes care*, vol. 10, no. 5, pp. 622–628, 1987.

[24] N. Demitri and A.M. Zoubir, "A robust kernel density estimator based mean-shift algorithm," in *2014 IEEE International Conference on Acoustics, Speech and Signal Processing (ICASSP)*, May 2014, pp. 7964–7968.